ARID ZONE JOURNAL OF ENGINEERING, TECHNOLOGY & ENVIRONMENT
AZOJETE September 2023. Vol. 19(3):505-518
Published by the Faculty of Engineering, University of Maiduguri, Maiduguri, Nigeria.
Print ISSN: 1596-2490, Electronic ISSN: 2545-5818
www.azojete.com.ng

ORIGINAL RESEARCH ARTICLE

INVESTIGATING THE EFFECTS OF DIBORON TRIOXIDE ON ZINC SILICATE-BASED GLASS-CERAMIC DERIVED FROM WASTE SODA LIME SILICA FOR POTENTIAL PHOSPHOR MATERIALS APPLICATION

I. M. Alibe[1]*, S. Nasir[2], M. H. M. Zaid[3], and A. M. Alibe[4]

[1]*Mechanical Engineering Department, Faculty of Engineering and Technology, Nigerian Army University Biu. No. 1, Gombe Road, PMB 1500, Biu, Borno State.*
[2]*Department of Chemistry, Faculty of Science, Federal University Dutse, P.M.B. 7156, Dutse, Jigawa State.*
[3]*Department of Physics, Faculty of Science, Universiti Putra Malaysia, 43400 UPM Serdang, Selangor, Malaysia*
[4]*Mechanical Engineering Departments, Federal Polytechnic Damaturu, Yobe State Nigeria.*

**Corresponding author's email address: babaiya l@gmail.com*

ARTICLE INFORMATION

Submitted 10 April, 2023
Revised 7 June, 2023
Accepted 10 June, 2023

Keywords:
Glass-ceramic
Melt-quenching
Waste SLS glass
Band gap energy
Amorphous

ABSTRACT

Over the last few decades, researchers have developed great deals of interest focusing on the fabrication and synthesis of zinc silicate-based glass-ceramic. However, using waste materials as precursors for the fabrication is yet another milestone in waste management. Thus, in this study, zinc silicate glass-ceramic was fabricated using sola lime silica (SLS) glass waste as a source of silicon. The series of precursor glass in the $(ZnO)_{0.6-x}\ (B_2O_3)_x\ (SLS)_{0.4}$ *system was prepared by the conventional solid-state melt-quench technique through a controlled crystallization process. The physical, structural, and optical properties of the glass system were obtained by density measurement, X-Ray diffraction, Fourier Transform Infrared Spectroscopy, Ultraviolet-visible spectroscopy, respectively. The density of the* $(ZnO)_{0.6-x}\ (B_2O_3)_x\ (SLS)_{0.4}$ *glasses series was observed to be decreasing with the increment of* $wt.\%\ B_2O_3$ *content. The XRD spectra of the* $(ZnO)_{0.6-x}\ (B_2O_3)_x\ (SLS)_{0.4}$ *samples with 0 and 0.01 wt.%* B_2O_3*, exhibits major diffraction peaks attributed to the ZnO phase in the glass matrix. However, as* B_2O_3 *content increased, the precursor glass sample shown by the XRD spectra depicted a broad halo characteristic, which reflected the properties of amorphous glass that were observed at the composition of 0.05 wt.%* B_2*. From FTIR spectra, the bands at 500, 688, 902 and 1243* cm^{-1} *can be associated with stretching vibrations of* ZnO_4 *and Si-O-B bending vibrations, stretching vibration of the B–O bonds in the* BO_4 *units, and modes of boron–oxygen triangular* BO_3 *units. The intensity of the IR band increases with increasing percentage of* B_2O_3*. The UV-Vis analysis of the samples with 0 and 0.01 wt.%* B_2O_3 *demonstrates crystalline hump and varies at 370 nm. It was observed that the addition of* B_2O_3 *to the ZnO-SLS glass network caused the glassy amorphous state with an absence of a sharp absorption edge at 0.05, 0.10, and 0.15 wt.%* B_2O3*.The* $(ZnO)_{0.6-x}\ (B_2O_3)_x\ (SLS)_{0.4}$ *system shows increase in band gap when the composition of* B_2O_3 *increased. When* ZnO *serves as a modifier, the number of NBOs will increase, and this will cause the expansion of glass network. The zinc silicate-based glass-ceramic produced has been classified to be a semiconductor due to the wide optical band gap energy obtained and may have key potential applications for future LED and other optoelectronic lighting devices.*

1.0 Introduction

Researchers in the past decade have shown significant interest on optoelectronics advanced materials such as transition metal-based silicate glass and glass-ceramics (Brugger et al., 2003; Takesue et al., 2009; Mondillo et al., 2020). These materials are used mostly as phosphor host for light-emitting diodes (LED), photodetectors, semiconductor lasers and other optoelectronic applications (Oueslati-Omrani & Hamzaoui, 2020). It is imperative to note that glasses that are silicate based especially those produced with larger content of ZnO are of great interest for numerous applications from conventional glasses and glass ceramics to an advanced performance optical glass (Oueslati-Omrani and Hamzaoui., 2020). Willemite, also known as zinc silicate (Zn_2SiO_4), is renowned for its suitability as a good host glass material used for several guest ions of rare–earth and transitional metals to attain higher effectiveness in displaying a wider range of multi–colours for luminescence application (Omri et al., 2013; El Mir and Omri, 2014; Al–Nidawi et al., 2017; Effendy et al., 2017; Zaid et al., 2016; Omar et al., 2017; Omar et al., 2016a; Rasdi et al., 2017;). For instance, the luminescence characteristics of rare earth ions (RE^{3+}) like the long emission lifetime, sharper luminescence array and the characteristic spectral behavior as they are filled by 4f shells and shielded by the outer $5s^2$ and $5p^6$ orbitals are some of the motivating drivers for their choice in nowadays optoelectronic application. For this reason, willemite doped with RE^{3+} is creating major attention for its luminescence efficiency and colour purity for lighting devices (Omar et al., 2016b; Omar et al., 2017). Furthermore, in the last decade, Takesue et al. (2009) reported the optical performance of willemite doped manganese (Zn_2SiO_4:Mn^{2+}) phosphors where the $3d^5$ electron transition in Mn^{2+} ions is characterized as activating centre in the structure. The rigid lattice structure (noncentrosymmetric cationic sites) of willemite made it a host material of choice for excellent performance in lighting devices and optoelectronic applications (Abdel-Hameed & Marzouk, 2022; Wei et al., 2022).

Previously, several researchers over the past decade reported different techniques used for the fabrication of willemite-based phosphor (Takesue et al., 2009). These techniques include, but are not limited to hydrothermal (Samigullina et al., 2017), polymer sonochemical (Masjedi-Arani & Salavati-Niasari, 2016), sol–gel (Benchikhi et al., 2022), spray pyrolysis (Kusdianto et al., 2020), and simple thermal treatment (Alibe et al., 2021). Nevertheless, other researchers observed that some of the processes are not time-effective and often involve complicated synthesis procedures that are financially expensive. Optionally, the conventional method, like the solid-state sintering method, offers a better alternative for cost-effective production, a shorter period of the procedure, and large-scale production of the material (Sarrigani & Amiri, 2019). Furthermore, obtaining silica (SiO_2) sources from a complex chemical process mentioned earlier seems to be expensive and consumes time, yet little amount is produced through the process (Takesue et al., 2009). Therefore, the use of another sources especially one which the precursor is obtained from waste recycled material is encouraged. Example of such is the waste from soda–lime–silica glass (SLS) which is commonly used glass and could be obtained in our surroundings (Sarrigani & Amiri, 2019). The spread of damage glasses disposal by the glass manufacturing industries has caused the SLS based glasses to become a huge pollutant to the environment. To curb the menace, several

Corresponding author's e-mail address: babaiya1@gmail.com

scientist tend to convert and used the waste SLS glass as a source of silica in the research (Zaid et al., 2016; Omar et al., 2017; Effendy et al., 2017;Wei et al., 2022). Interestingly, this goes with waste-to-wealth creation and also offers a better cost-effective manufacturing. Besides, the incorporation of SLS glass waste in the willemite formation can also lower its melting point, improve the clarity as well as enhance thermal and chemical stability of the final material produced (Takesue et al., 2009; Wei et al., 2022). Oxide-based glass formers often add on to the bulk matrix to enhance the formation of a glass and form the interconnected backbone of the glass network. One of the most studied glass former over the decade is the Boron oxide (B_2O_3) (Li et al., 2013). Previous literature suggest that the addition of little quantity of B_2O_3 could improve and stabilize the disorder in matrix and further serve as a nucleation agent to hasten crystallization process (Hamnabard et al., 2012; Li et al., 2013; Qazvini et al., 2012).

In this work, new approach was proposed to fabricate willemite glass-ceramic derived from ZnO–B2O3–SLS glass system. The influence of calcination temperature on the phase structural formation, and optical emission properties were thoroughly discussed.

2.0 Materials and Methods

2.1 Materials Preparation

This section describes the glass preparation process for the work according to the solid state technique (Zaid et al., 2016; Omar et al., 2017; Effendy et al., 2017;) . The precursors used were SLS glass, ZnO, and B_2O_3. The SLS glass powder was prepared from waste broken glasses obtained from the dumping site, while the ZnO and B_2O_3 powders were purchased from Sigma-Aldrich and used without further purification. The $(ZnO)_{0.6-x}\,(B_2O_3)_x\,(SLS)_{0.4}$ glasses samples were prepared using the conventional melt-quenching technique for glass production. The SLS glass waste was at first crushed to form glass powder and sieved to 45 μm particle size. The SLS glass powder obtained was combined with ZnO and B_2O_3 using the composition mixture of $(ZnO)_{0.6-x}\,(B_2O_3)_x\,(SLS)_{0.4}$ in weight percent. The mixed sample was allowed to undergo a milling process by placing them into a milling jar and running them for 30 minutes in a Ball Milling Machine with 50 rpm to ensure homogeneity of the mixture and control the size distribution of the composition. The milling process was followed by melting about 30 g of the milled sample at a temperature of 1450 °C for 2 h. When melting point is achieved, the hot sample is then quenched in a container filled with water to produce glass frits. Due to the fast quenching process, the glass frits produced were transparent devoid of bubbles. The earlier process of crushing, grinding, and sieving the glass frits produced a fine glass powder with an average particle size of 45 μm for the pelleting process. Note that pelletizing is the process of compressing or molding a material into the shape of a pellet. Therefore, after the sieving process, the sample was mixed with 1.75 weight percent of polyvinyl alcohol (PVA), which served as a binding agent, and pressed using a hydraulic press machine until it reached 4 tons/m^2. Each sample was left for 10 minutes to form 13 mm diameter glass pellets. The solid pellets were all sintered at 700 °C for 2

Corresponding author's e-mail address: babaiya1@gmail.com

hours to decompose the PVA. A constant heating rate of 10 °C/min was maintained throughout. Subsequently, all the samples obtained were characterized using densimeter and vernier caliper measurements to determine their physical properties. The structural properties of the glass formed were studied using X-ray diffraction (XRD) (PW 3040/60 model, Philips, San Jose, CA, USA) and Fourier transform infrared reflection (FTIR) (Spectrum 100 model, Perkin Elmer; Waltham, Massachusetts, USA). The optical properties were analysed using ultraviolet–visible (UV–Vis) (UV-3600 model, Shimadzu, Kyoto, JAPAN) and photoluminescence (PL) (LS 55 model, Perkin Elmer, Waltham, Massachusetts, USA) spectroscopic techniques, respectively.

2.2 Characterization

In this work, all samples obtained were characterized for their physical properties using densimeter and vernier caliper measurements. The structural properties of the glass formed were studied using X-ray diffraction (XRD) (PW 3040/60 model, Philips, San Jose, CA, USA), Fourier transform infrared reflection (FTIR) (Spectrum 100 model, Perkin Elmer; Waltham, Massachusetts, USA), and optical properties were analysed using ultraviolet–visible (UV–Vis) (UV-3600 model, Shimadzu, Kyoto, JAPAN) and photoluminescence (PL) (LS 55 model; Perkin Elmer; Waltham, Massachusetts, USA) spectroscopic techniques respectively (Omri et al., 2013; Zaid et al., 2016a; Rasdi et al., 2017; Effendy et al., 2017).

In glass and glass ceramic-based research, the physical properties of the material, such as its density, are considered as an important factor in determining the material's strength. The density was obtained by using densitometer MS-300S in order to determine the molecular packing inside the sample (Samsudin et al., 2016). Ethanol was used as an immersion liquid in this experiment, which was repeated three (3) times in order to avoid parallax error and mathematically shown in the equation.

$$\rho_{=}\frac{m}{V} \qquad (1)$$

Where ρ is the density of sample $(\mathrm{g\,cm}-3)$, m is the mass of pellet (g) and V is the volume of ethanol (cm^{-3}).

3.0 Results and Discussion

This section analyses and discussed comprehensively the data obtained from the characterization of the samples.

3.1 *Density and Linear Shrinkage Analysis*

Table 1 shows the density of five glass samples respectively. The Series of $(ZnO)_{0.6-x}\,(B_2O_3)_x\,(SLS)_{0.4}$ glasses were observed to be decreasing with the increment of B_2O_3 content. The data measurement shows the trend of density samples decrease with increasing weight fraction of B_2O_3 as expressed graphically in Figure 1. It is noteworthy that this decrement in density of the glass samples was due to lower B_2O_3 atomic mass compared to

other element in glass system. The atomic mass of B_2O_3 is 69.617 amu which is lower as compared to atomic mass of ZnO (81.38 amu). This phenomenon led to the decrease in density from 2.80 to 2.50 g cm^{-3} as ZnO content decrease from 0.6 to 0.455 w.t%.

Table 1: The compositions and density of the glasses for $(ZnO)_{0.6-x}\ (B_2O_3)_x\ (SLS)_{0.4}$

Samples	Compositions	Density
1	$(ZnO)_{0.6}\ (SLS)_{0.4}$	2.80
2	$(ZnO)_{0.59}\ (B_2O_3)_{0.01}\ (SLS)_{0.4}$	2.72
3	$(ZnO)_{0.55}\ (B_2O_3)_{0.05}\ (SLS)_{0.4}$	2.60
4	$(ZnO)_{0.50}\ (B_2O_3)_{0.10}\ (SLS)_{0.4}$	2.52
5	$(ZnO)_{0.45}\ (B_2O_3)_{0.15}\ (SLS)_{0.4}$	2.50

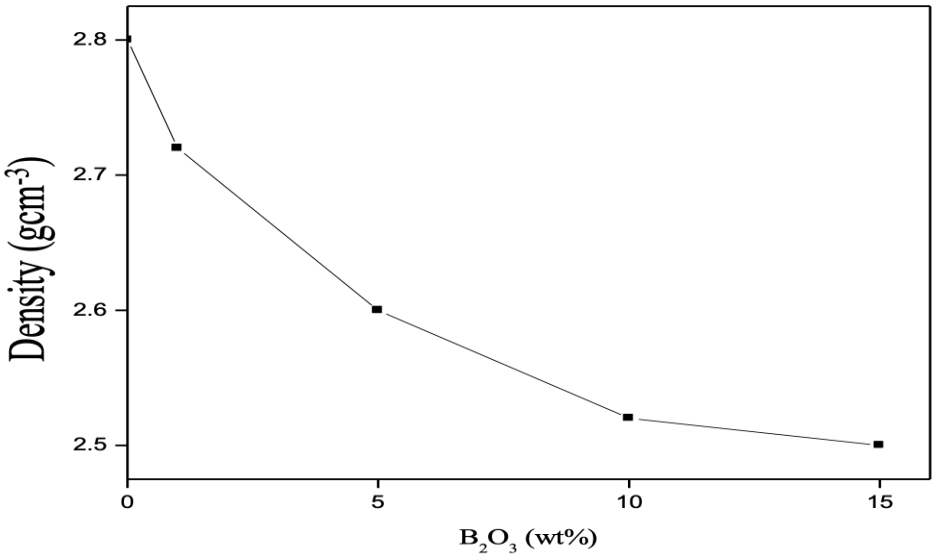

Figure 1. Density of $(Zno)_{(0.6-X)}\ (B_2O_3)_X\ (SLS)_{0.4}$ glasses

3.2 XRD Structure and Phase Analysis

The structure of the prepared glasses samples were analyzed using XRD. Figure 2 shows a XRD pattern of $(ZnO)_{0.6-x}\ (B_2O_3)_x\ (SLS)_{0.4}$ based glass samples. The presence of ZnO phase in the glass matrix was observed in the samples with 0 and 0.01 wt.% B_2O_3. By matching the diffraction peaks in the pattern with the standard diffraction pattern of the XRD, the sample with 0 wt.% B_2O_3 exhibit 8 major diffraction peaks of ZnO at 31.97°, 34.65°, 36.46°, 47.75°, 56.79°, 63.07°, 68.14° and 69.27° corresponding to (0 1 0), (0 0 2), (2 2 0), (0 1 2), (1 1 0), (0 1 3), (1 1 2) and (0 2 1) planes. While, the sample with 0.01 wt.% B_2O_3 also exhibit 6 major diffraction peaks at 31.87°, 34.54°, 36.37°, 56.76°, 63.05°, and 68.14° respectively (Shofria et al., 2010).

It appears that when little quantity of the B_2O_3 is substituted for ZnO, the glass structure may form a crystalline phase as depicted in Figure 2. It was reported by some authors that the glass

network modifier work as a crystallization promoting agent, thereby providing nucleation positions arising from effect on the glass stability, caused by ion substitution within the glass network (Qazvini et al., 2012; Sarrigani and Amiri 2019). In addition, Takesue et al., 2009 reported that ZnO work as a network modifier that breaks the bonds between oxygen and glass former ions, which may lead to a change in the structural unit that affects the physical characteristics of the glass network. Thus, forms a non-bridging oxygens (NBO), as proved in samples with compositions of 0 and 0.01 wt.% B_2O_3. Besides, the high amount of ZnO can lead to more intense crystallization and favor the precipitation of optically active crystalline phases (Zaid et al., 2016a). Moreover, it show that there is very slight increase in the intensity of the diffraction peaks with the increment of ZnO content because the ratio of composition is not stable to achieve the amorphous phase (Zaid et al., 2016a). However, as B_2O_3 content increased, the precursor glass sample showed a broad halo characteristic, which reflected the properties of amorphous glass that were observed at a the composition of 0.05 wt.% B_2O_3 (Mohd Shofri et al., 2020). From the pattern, there is no discrete sharp peak, which implies the samples were fully in glass form. The amorphous hump was obtained at 33°. By comparing the increment of B_2O_3 in the glass system, it was observed that the peaks get broadened in the spectrum due to variation in the inter-atomic distances (Shofria et al., 2010). It was confirmed and also reported by Lim et al. (2002), that the formation of covalent B-O bonding produced a stronger, better chemically resistant glass network with higher packing density and lower crystallization tendency (Mohd Shofri et al., 2020; Shofria et al., 2010).

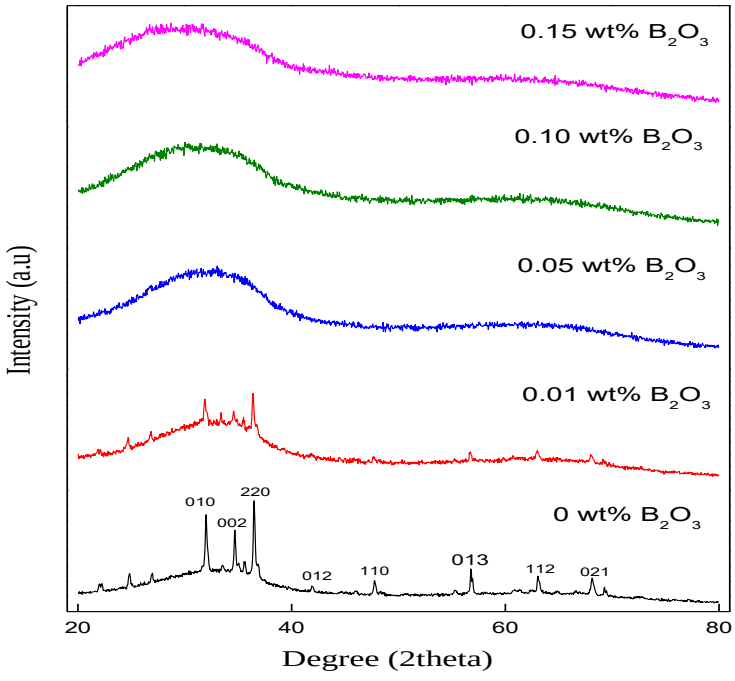

Figure 2. XRD Pattern of $(ZnO)_{(0.6-x)}$ $(B_2O_3)x$ $(SLS)_{0.4}$ glasses

3.3 FTIR Analysis

All the functional groups and the existing chemical bonding in the Pattern of $(ZnO)_{(0.6-x)}$ $(B_2O_3)_x$ $(SLS)_{0.4}$ glasses were assessed by FTIR analysis a shown in table 2 and figure 3 respectively. The structure of the glass samples were measured using FTIR in the wavenumber range of 280 to 4000 cm^{-1}. The IR spectrum is divided into two paths; the first one consists of the main sharp, distinctive and characteristic absorption bands extending in the mid IR region from 400 to about 1400 cm^{-1}, and the second part reveals only small peaks from 1400 to 4000 cm^{-1}. Furthermore, silicate glass structure having disordered geometry with the formation of tetrahedral coordination of BO_4 units among oxide glasses. According to the glass formation theory, the oxides of metal cation (e.g. Zn^{2+}) with valence one or two plays an important role as glass modifier (Hivrekar et al., 2017). Some of the bridging oxygen of tetrahedral BO_4 units combines with glass modifier coordinated by six, eight or even more oxygen atom to form glass network with non-bridging oxygen (De Leede & De Waal, 1988). Figure 3 shows the samples analysed and was obtained at the range of 400-1400 cm^{-1} which signifies the vibrations of main building units of SLS. Then, it was obvious that the band at 500, 688, 902 and 1243 cm^{-1} can be associated stretching vibrations of ZnO_4 units (Zaid et al., 2016b) and Si-O-B bending vibrations, stretching vibration of the B–O bonds in the BO_4 units and modes of boron–oxygen triangular BO_3 units (Kullberg et al., 2017). The intensity of IR band become higher with increasing percentage of B_2O_3 (Mohd Shofri et al., 2020).

Table 2: IR absorption bands and band assignment (Kullberg et al., 2017)

Wavenumber (cm^{-1})	**Assignment of vibrational mode**
500	Stretching vibrations of ZnO_4 units
650 – 700	Si-O-B bending vibrations
840 – 930	Stretching vibration of the B–O bonds in the BO_4 units
1234 – 1250	Modes of boron–oxygen triangular BO_3 units

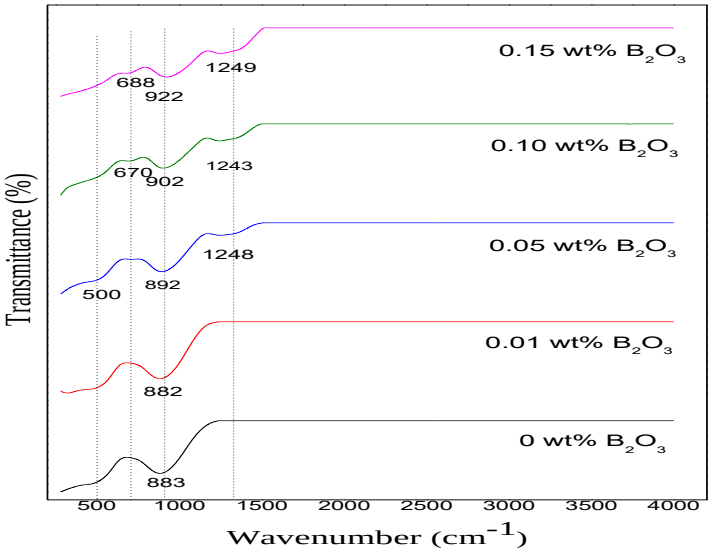

Figure 3: FT-IR spectra of sample $(ZnO)_{0.6-x}\ (B_2O_3)_x\ (SLS)_{0.4}$ glasses

3.3 UV-VIS Analysis

The absorption spectra of sample $(SLS)_{0.4}\ (ZnO)_{0.6-x}\ (B_2O_3)_x$ glasses are presented in Figure 4. Ultra violet regions are very important in study field as it provides scientist with information to understand the electronic band gap of a particular material and to find the optical absorbance whether it bands at high or shorter wavelength. Optical absorbance is higher at lower wavelength region while lower at higher wavelength region whereas ultraviolet "cut off" emerge as a term to describe increase in absorption factor spectra (Singh et al., 2008).

Figure 4 shows that samples with 0 and 0.01 wt.% B_2O_3 has crystalline hump which varies at 370 nm. It was observed after the addition of B_2O_3 to ZnO-SLS glass network has caused the glassy amorphous state with absence of shrill absorption edge at 0.05, 0.10 and 0.15 wt.% B_2O_3. Moreover, the absorption edge (cut-off wavelength) tends to move to higher wavelength sides when the amount of B_2O_3 increases in the glass system and produces a non-sharp structure due to the disorder in the matrix. It is clear that there is no sharp absorption edge after addition of 0.05, 0.10 and 0.15 wt.% B_2O_3. This corresponds to the characteristics of the glassy state.

Basically, there are two transitions occurring in the energy band gap of materials, these are direct allowed or indirect allowed transition which can occurs regardless of crystalline or amorphous material of the glass. These transitions usually occur during the reaction among electromagnetic wave when it reacts with electrons at the valence state thus forcing it to be promoted to the conduction state (Gnutzmann and Clausecker, 1974). In order to find different kinds of transition, the values n=1/2 and n=2 which are for direct allowed and indirect forbidden transitions were substituted into $(\alpha hv)^{\frac{1}{n}}$ against photon energy (hv) and plots were displayed by extrapolating the linear region of the curve as shown in Figure 5 and 6 respectively. By comparing the value of

direct forbidden and indirect allowed transition with different composition for $(SLS)_{0.4}\ (ZnO)_{0.6-x}\ (B_2O_3)_x$ glass system obtained using different values of n, a good agreement with E_{opt} values for n=2 is the best transition. It also can be resolved that optical band gap obtained for $(SLS)_{0.4}\ (ZnO)_{0.6-x}\ (B_2O_3)_x$ glass favors indirect forbidden transition (n=2). Table 3 shows the calculated band gap energy. The samples shows increase in band gap when the composition of B_2O_3 increases. When ZnO serves as a modifier, the number of NBOs will increase and this will cause the expansion of glass network. Increase in optical band gap clearly state that the glass has higher number of NBO's rather than BO's.

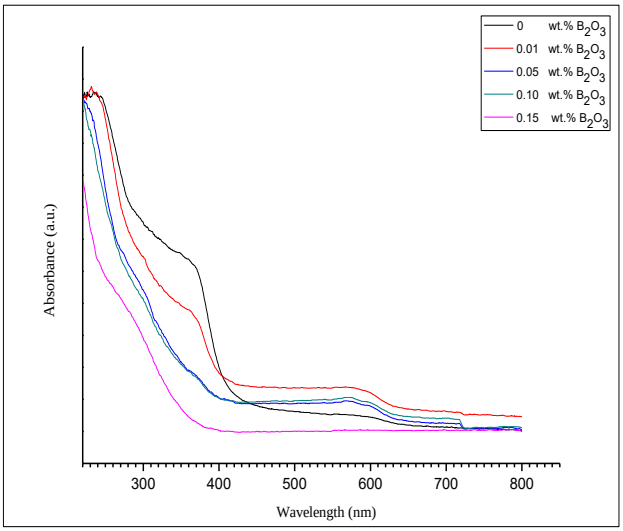

Figure 4: Absorption spectra of sample $(ZnO)_{0.6-x}\ (B_2O_3)_x\ (SLS)_{0.4}$ glasses

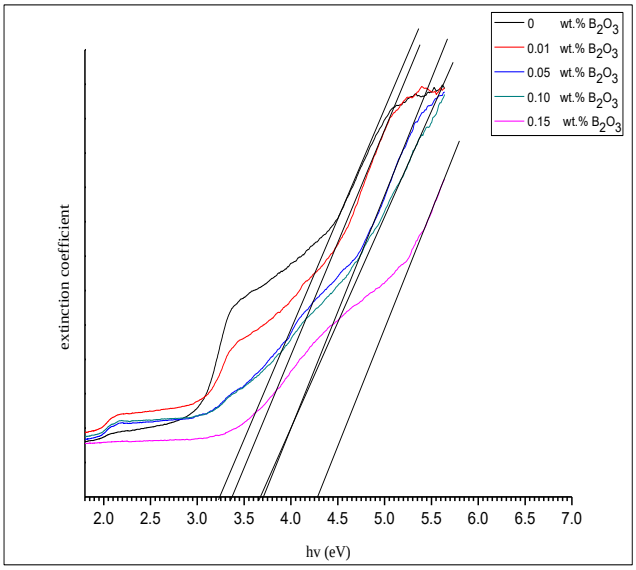

Figure 5: plot of $(\alpha hv)^{\frac{1}{2}}$ as a function of energy for $(ZnO)_{0.6-x}\ (B_2O_3)_x\ (SLS)_{0.4}$ glasses, n=2

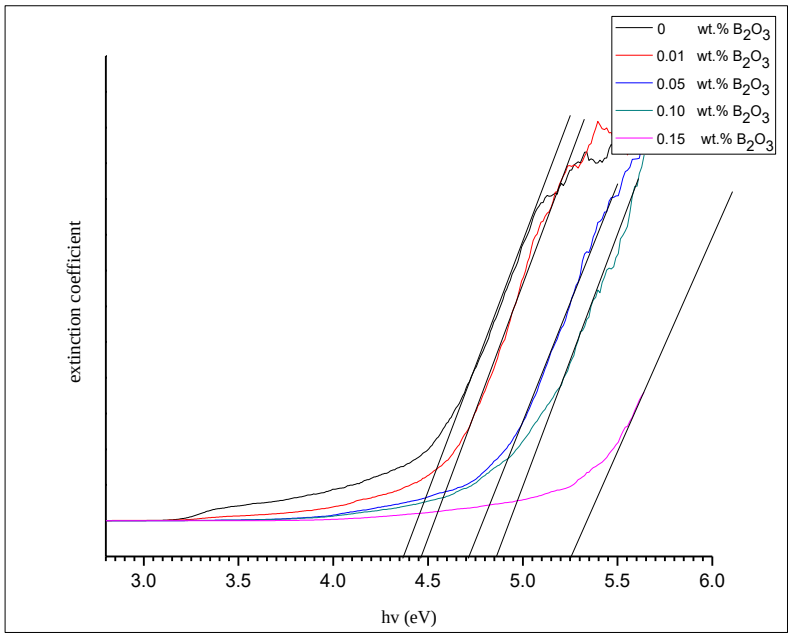

Figure 6: plot of $(\alpha hv)^2$ as a function of energy for $(ZnO)_{0.6-x}\ (B_2O_3)_x\ (SLS)_{0.4}$, n=1/2

Table 3: Energy Band Gap (eV) for $(ZnO)_{0.6-x}\ (B_2O_3)_x\ (SLS)_{0.4}$ glass system

Samples	Direct allowed transition, n=1/2	Indirect forbidden transition, n=2
$(ZnO)_{0.60}\ (SLS)_{0.4}$	4.35	3.25
$(ZnO)_{0.59}\ (B_2O_3)_{0.01}\ (SLS)_{0.4}$	4.45	3.35
$(ZnO)_{0.55}\ (B_2O_3)_{0.05}\ (SLS)_{0.4}$	4.70	3.60
$(ZnO)_{0.45}\ (B_2O_3)_{0.10}\ (SLS)_{0.4}$	4.85	3.65
$(ZnO)_{0.40}\ (B_2O_3)_{0.15}\ (SLS)_{0.4}$	5.25	4.30

Corresponding author's e-mail address: babaiya1@gmail.com

4.0 Conclusions

Based on this study, the ZNO–B_2O_3–SLS glass system had been successfully fabricated and investigated. The physical, structural, and optical properties of glass system were comprehensively discussed. The density of the material was observed to decrease as the B_2O_3 content is increased. This is attributed to the lower atomic mass of B_2O_3 compared to ZNO and SiO_2 present in the glass system. The functional groups attached to the glass system observed from the ftir spectrum reveal that the ir spectrum is divided into two paths; the first one consists of the main sharp, distinctive and characteristic absorption bands extending in the mid ir region from 400 to about 1400 cm^{-1}, and the second part reveals only small peaks from 1400 to 4000 cm^{-1}. It was obvious that the bands at 500, 688, 902 and 1243 cm^{-1} can be associated with stretching vibrations of ZNO_4 units, Si-O-B bending vibrations, stretching vibration of the b–o bonds in the bo_4 units, and modes of boron–oxygen triangular bo_3 units. The band gap characteristics of the glass system favor direct and indirect forbidden transitions, and the increase in the b_2o_3 content causes higher absorption in the uv region, thus resulting in a lower band gap. Based on this study, B_2O_3 served as an important glass formers and flux materials that connects the backbone of the glass network. The findings in this work open the path to comprehend the effects of b_2o_3 content on the structural and optical properties of the ZNO–B_2O_3–SLS glass system, and the wide band gap energy of the material obtained may have key potential applications for future led and other optoelectronic lighting devices.

Conflict of Interests

The authors declare that there is no conflict of interests regarding the publication of this paper.

Acknowledgments

The researchers gratefully acknowledge the financial support for this study from the Malaysian Ministry of Higher Education (MOHE) and Universiti Putra Malaysia through the Fundamental Research Grant Scheme (FRGS) and Inisiatif Putra Berkumpulan (IPB) research grant. The researchers would like to gratefully acknowledge Associate Professor Khamirul Amin Matori (Department of Physics, Faculty of Science, Universiti Putra Malaysia) for providing the Laboratory tools and equipment used in the research work.

References

Abdel-Hameed, SAM. and Marzouk, M.A. 2022. Long afterglow from multi dopant transparent and opaque glass ceramic phosphor for white, red, yellow, and blue emissions: Zn_2SiO_4: Eu^{3+}, Dy^{3+}, Mn^{2+}. Journal of Alloys and Compounds, 893: 162337.

Alibe, IM., Matori, KA., Zaid, MHM., Nasir, S., Alibe, AM. and Khiri, MZA. 2021. Polymer Thermal Treatment Production of Cerium Doped Willemite Nanoparticles: An Analysis of Structure, Energy Band Gap and Luminescence Properties. Materials, 14(5):1118.

Corresponding author's e-mail address: babaiya1@gmail.com

Al-Nidawi, AJA., Matori, KA., Zakaria, A. and Zaid, MHM. 2017. Effect of MnO_2 doped on physical, structure and optical properties of zinc silicate glasses from waste rice husk ash. Results in Physics, 1(7): 955–961.

Benchikhi, M., Hattaf, R., Moutaabbid, A. and El Ouatib, R. 2022. Structural, morphological, and optical properties of Co-substituted Zn_2SiO_4 nanopowders prepared by a hydrothermal-assisted sol-gel process. Materials Chemistry and Physics, 276(1): 125434.

Brugger, J., McPhail, DC., Wallace, M. and Waters, J. 2003. Formation of willemite in hydrothermal environments. Economic Geology, 98(4):819-835.

De Leede, G., and De Waal, H. 1988. Evaluation of glass formation criteria. Journal of Non-Crystalline Solids, 104(1): 45–51.

Effendy, N., Wahab, ZA., Abdul Aziz, SH., Matori, KA., Zaid, MHM. and Rashid, SSA. 2017. Characterization and optical properties of erbium oxide doped ZnO–SLS glass for potential optical and optoelectronic materials. Materials Express, 7(1): 59–65.

El Mir, L. and Omri, K. 2014. Photoconversion from UV-to-yellow in Mn doped zinc silicate nanophosphor material. Superlattices and Microstructures, 75: 89–98.

Gnutzmann, U. and Clausecker, K. 1974. Theory of direct optical transitions in an optical indirect semiconductor with a superlattice structure. Applied Physics, 3(1): 9–14.

Hamnabard, Z., Khalkhali, Z., Qazvini, SSA., Baghshahi, S. and Maghsoudipour, A. 2012. Preparation, heat treatment and photoluminescence properties of V-doped $ZnO–SiO_2–B_2O_3$ glasses. Journal of Luminescence, 132(5):1126–1132.

Hivrekar, MM., Sable, DB., Solunke, MB. and Jadhav, KM. 2017. Network structure analysis of modifier CdO doped sodium borate glass using FTIR and Raman spectroscopy. Journal of Non-Crystalline Solids, 474:58–65.

Kullberg, AT., Lopes, AA., Veiga, JP. and Monteiro, RC. 2017. Crystal growth in zinc borosilicate glasses. Journal of Crystal Growth, 457:239–243.

Kusdianto, K., Widiyastuti, W., Shimada, M., Qomariyah, L. and Winardi, S. (2020). Fabrication of $ZnO-SiO_2$ nanocomposite materials prepared by a spray pyrolysis for the photocatalytic activity under UV and sunlight irradiations. IOP Conference Series: Materials Science and Engineering, 778(1): 012105.

Li, HC., Wang, DG., Hu, JH. and Chen, CZ. 2013. Effect of the partial substitution of K_2O, MgO, B_2O_3 for CaO on crystallization, structure and properties of $Na_2O–CaO–SiO_2–P_2O_5$ system glass-ceramics. Materials Letters, 106: 373–376.

Lim, SG., Kriventsov, S., Jackson, TN., Haeni, JH., Schlom, DG., Balbashov, AM., Uecker, R., Reiche, P., Freeouf, JL. and Lucovsky, G. 2002. Dielectric functions and optical bandgaps of high–

K dielectrics for metal–oxide–semiconductor field–effect transistors by far ultraviolet spectroscopic ellipsometry. Journal of Applied Physics, 91(7): 4500–4505.

Masjedi-Arani, M. and Salavati-Niasari, M. 2016. A simple sonochemical approach for synthesis and characterization of Zn2SiO4 nanostructures. Ultrasonics Sonochemistry, 29:226–235.

Mondillo, N., Accardo, M., Boni, M., Boyce, A., Herrington, R., Rumsey, M. and Wilkinson, C. 2020. New insights into the genesis of willemite (Zn_2SiO_4) from zinc nonsulfide deposits, through trace elements and oxygen isotope geochemistry. Ore Geology Reviews, 118:103307.

Mohd Shofri, MFS., Mohd Zaid, MH., Matori, KA., Fen, YW., Yaakob, Y., Jaafar, SH., Wahab, SAA. and Iwamoto, Y. 2020. Phase Transformation, Optical and Emission Performance of Zinc Silicate Glass-Ceramics Phosphor Derived from the ZnO–B_2O_3–SLS Glass System. Applied Sciences, 10(14): 4940.

Omar, NAS., Fen, YW. and Matori, KA. 2016a. Photoluminescence properties of Eu^{3+}-doped low cost zinc silicate based glass ceramics. Optik-International Journal for Light and Electron Optics, 127(8): 3727–3729.

Omar, NAS., Fen, YW. and Matori, KA. 2017. Europium doped low cost Zn_2SiO_4 based glass ceramics: A study on fabrication, structural, energy band gap and luminescence properties. Materials Science in Semiconductor Processing, 61:27–34.

Omar, NAS., Fen, YW., Matori, KA., Zaid, MHM. and Samsudin, NF. 2016b. Structural and optical properties of Eu3+ activated low cost zinc soda lime silica glasses. Results in Physics, 6: 640–644.

Omri, K., El Ghoul, J., Alyamani, A., Barthou, C. and El Mir, L. 2013. Luminescence properties of green emission of SiO_2/Zn_2SiO_4:Mn nanocomposite prepared by sol–gel method. Physica E: Low-Dimensional Systems and Nanostructures, 53: 48–54.

Omri, K., Najeh, I., Dhahri, R., El Ghoul, J. and El Mir, LJME. 2014. Effects of temperature on the optical and electrical properties of ZnO nanoparticles synthesized by sol–gel method. Microelectronic Engineering, 128: 53-58.

Oueslati-Omrani, R. and Hamzaoui, AH. 2020. Effect of ZnO incorporation on the structural, thermal and optical properties of phosphate based silicate glasses. Materials Chemistry and Physics, 242: 122461.

Qazvini, SSA., Hamnabard, Z., Khalkhali, Z., Baghshahi, S. and Maghsoudipour, A. 2012. Photoluminescence and microstructural properties of SiO2–ZnO–B2O3 system containing TiO_2 and V_2O_5. Ceramics International, 38(2):1663–1670.

Rasdi, NM., Fen, YW., Omar, NAS., and Zaid, MHM. 2017. Effects of cobalt doping on structural, morphological, and optical properties of Zn_2SiO_4 nanophosphors prepared by sol-gel method. Results in Physics, 7:3820-3825.

Samigullina, RF., Tyutyunnik, AP., Gracheva, IN., Krasnenko, TI., Zaitseva, NA. and Onufrieva, TA. 2017. Hydrothermal synthesis of α-Zn2SiO4:V phosphor, determination of oxidation states and structural localization of vanadium ions. Materials Research Bulletin, 87:27–33.

Sarrigani, GV. and Amiri, IS. 2019. Literature Review of Glass-Ceramic and Willemite Production from Waste Materials. Willemite-Based Glass Ceramic Doped by Different Percentage of Erbium Oxide and Sintered in Temperature of 500-1100C, 13–27.

Samsudin, NF., Matori, KA., Fen, Y.W., Chyi, JL. Y., Omar, NAS., and Alassan, ZN. 2016. Optical and structural properties of Zn_2SiO_4:Mn^{2+} from SLS waste bottle obtained by a solid state method. Procedia Chemistry, 19: 57-67.

Shofria, MFSM., Zalamina, SNF., Matori, KA., Fen, YW., and Zaida, MHM. 2010. Physical, Structural, and Optical Properties of Zinc Silicate Based Glass-Ceramic Derived from ZnO-B_2O_3-SLS Glass System. Editors: Assoc. Prof. Dr. Mohd Mustafa Awang Kechik, 130(2010):33.

Singh, D., Singh, K., Singh, G., Mohan, S., Arora, M., and Sharma, G. 2008. Optical and structural properties of ZnO–PbO–B_2O_3 and ZnO–PbO–B_2O_3–SiO_2 glasses. Journal of Physics: Condensed Matter, 20(7):1-6.

Takesue, M., Hayashi, H., & Smith Jr, R. L. (2009). Thermal and chemical methods for producing zinc silicate (willemite): A review. Progress in Crystal Growth and Characterization of Materials, 55(3–4):98–124.

Wei, LZ., Mun, CW., Zakaly, HMH., Issa, SA., and Zaid, MHM. 2022. Influence of Sintering Duration on Crystal Phase and Optical Band Gap of Mn^{3+}-Doped Willemite-Based Glass-Ceramics. Journal of Electronic Materials, 51(3):1163–1168.

Zaid, MHM., Matori, KA., Ab Aziz, SH., Kamari, HM., Wahab, ZA., Effendy, N., and Alibe, IM. 2016a. Comprehensive study on compositional dependence of optical band gap in zinc soda lime silica glass system for optoelectronic applications. Journal of Non-Crystalline Solids, 449:107–112.

Zaid, M., Hafiz, M., Amin Matori, K., Abdul Aziz, SH., Kamari, HM., Yunus, M., Mahmood, W., Abdul Wahab, Z., and Samsudin, NF. 2016b. Fabrication and crystallization of ZnO-SLS glass derived willemite glass-ceramics as a potential material for optics applications. Journal of Spectroscopy, 2016:1-7.

Corresponding author's e-mail address: *babaiya1@gmail.com*